The American Journal of Pathology, Vol. 184, No. 10, October 2014

The American Journal of
PATHOLOGY
ajp.amjpathol.org

ANIMAL MODELS

Mutations in Pre-mRNA Processing Factors 3, 8, and 31 Cause Dysfunction of the Retinal Pigment Epithelium

Michael H. Farkas,* Deborah S. Lew,† Maria E. Sousa,* Kinga Bujakowska,*† Jonathan Chatagnon,† Shomi S. Bhattacharya,†‡§ Eric A. Pierce,* and Emeline F. Nandrot†

From the Ocular Genomics Institute, Department of Ophthalmology, Massachusetts Eye and Ear Infirmary, Harvard Medical School, Boston, Massachusetts; the Vision Institute,† INSERM, U968, Sorbonne Universités, UPMC Univ Paris 06, UMR_S 968, CNRS, UMR_7210, Paris, France; the Institute of Ophthalmology,‡ University College London, London, United Kingdom; and the Andalusian Center of Molecular Biology and Regenerative Medicine,§ Andalusian Center for Molecular Biology and Regenerative Medicine (CABIMER), Sevilla, Spain

Accepted for publication June 13, 2014.

Address correspondence to Emeline F. Nandrot, Ph.D., Institut de la Vision, Therapeutics Department, 17 rue Moreau, 75012 Paris, France; or Eric A. Pierce, M.D., Ph.D., Ocular Genomics Institute, Berman-Gund Laboratory, Department of Ophthalmology, Massachusetts Eye and Ear Infirmary, Harvard Medical School, 243 Charles St., Boston, MA 02114.
E-mail: emeline.nandrot@inserm.fr or eric_pierce@meei.harvard.edu.

Mutations in the ubiquitously expressed pre-mRNA processing factors 3, 8, and 31 (*PRPF3*, *PRPF8*, and *PRPF31*) cause nonsyndromic dominant retinitis pigmentosa in humans, an inherited retinal degeneration. It is unclear what mechanisms, or which cell types of the retina, are affected. Transgenic mice with the human mutations in these genes display late-onset morphological changes in the retinal pigment epithelium (RPE). To determine whether the observed morphological changes are preceded by abnormal RPE function, we investigated its phagocytic function in *Prpf3*$^{T494M/T494M}$, *Prpf8*$^{H2309P/H2309P}$, and *Prpf31*$^{+/-}$ mice. We observe decreased phagocytosis in primary RPE cultures from mutant mice, and this is replicated by shRNA-mediated knockdown of *PRPF31* in human ARPE-19 cells. The diurnal rhythmicity of phagocytosis is almost lost, indicated by the marked attenuation of the phagocytic burst 2 hours after light onset. The strength of adhesion between RPE apical microvilli and photoreceptor outer segments also declined during peak adhesion in all mutants. In all models, at least one of the receptors involved in binding and internalization of shed photoreceptor outer segments was subjected to changes in localization. Although the mechanism underlying these changes in RPE function is yet to be elucidated, these data are consistent with the mouse RPE being the primary cell affected by mutations in the RNA splicing factors, and these changes occur at an early age. *(Am J Pathol 2014, 184: 2641–2652; http://dx.doi.org/10.1016/j.ajpath.2014.06.026)*

The spliceosome is a ubiquitous, dynamic ribonucleoprotein macromolecule required for removing introns from a nascent RNA.[1] Mutations that cause autosomal dominant retinitis pigmentosa (RP) have been identified in five genes that encode proteins (PRPF3, PRPF6, PRPF8, PRPF31, and SNRNP200), which are found in the U4/U6.U5 tri–small nuclear ribonucleoprotein.[2] In aggregate, mutations in these genes are the second most common cause of dominant RP.[3–5] Defined by progressive, late-onset vision loss, RP is the most common form of inherited retinal degeneration, affecting approximately 1 in 3500 persons worldwide.[6] It is genetically heterogeneous and displays all three modes of Mendelian inheritance.[7] Affected tissues include the neural retina, retinal pigment epithelium (RPE), and choroid.[4] Because the components of the spliceosome are ubiquitously expressed in every cell type, it is not clear why mutations in these splicing factors cause only nonsyndromic RP. Further, the specific cell type(s) in the retina affected by these mutations has not yet been identified.

We have previously reported the characterization of mouse models of RNA splicing factor RP due to mutations in the *PRPF3*, *PRPF8*, and *PRPF31* genes, including *Prpf3*, *Prpf8*, and *Prpf31* knockout mice, and *Prpf3*-T494M and *Prpf8*-H2309P knockin mice.[8,9] On the basis of results from

Supported by the NIH National Eye Institute grants EY020902 (E.A.P., subaward to S.S.B. and E.F.N.) and F32-EY020747 (M.H.F.); Research to Prevent Blindness, United States; Agence Nationale de la Recherche, France, Chaire d'Excellence (S.S.B.); Fondation Voir et Entendre and Fondation Bettencourt Schueller Young Investigator grants (E.F.N.); Center National de la Recherche Scientifique (CNRS) (E.F.N.). In addition, the Institut de la Vision is funded by Institut National de la Santé et de la Recherche Médicale, France; Sorbonne Universités, Université Pierre et Marie Curie-Paris 6; Centre National de la Recherche Scientifique; and Département de Paris.

M.H.F. and D.S.L. contributed equally to this work.

E.A.P. and E.F.N. contributed equally as senior authors.

http://dx.doi.org/10.1016/j.ajpath.2014.06.026

studies of these mouse models and data from human studies, it is believed that mutations in *PRPF3* and *PRPF8* cause dominant disease via gain-of-function or dominant-negative mechanisms, whereas mutations in *PRPF31* cause disease via haploinsufficiency.[9–11] Morphological changes in the aging RPE, but not the neural retina, of the *Prpf3*-T494M and *Prpf8*-H2309P knockin mice and *Prpf31*$^{+/-}$ mice were of particular interest, in which we observed the loss of basal infoldings, the formation of basal deposits beneath the RPE, and vacuolization in the cytoplasm. These RPE degenerative changes were observed in heterozygous *Prpf3*$^{T494M/+}$, *Prpf8*$^{H2309P/+}$, and *Prpf31*$^{+/-}$ mice and were more pronounced in homozygous *Prpf3*$^{T494M/T494M}$ and *Prpf8*$^{H2309P/H2309P}$ knockin mice.[8]

The RPE is vital for the overall well-being of the retina.[12] The daily elimination of spent photoreceptor outer segment (POS) extremities is a highly coordinated process, and phagocytosis of shed POS extremities occurs on a rhythmic basis.[13] Some receptors implicated in POS phagocytosis also participate in overall retinal adhesion and its physiological rhythm.[14] Peak phagocytosis and retinal adhesion occur approximately 2 and 3.5 hours after light onset, respectively, and are at their minimum levels roughly 10 hours later.[13–15] The RPE is a professional macrophage in which binding and internalization of a substrate is coordinated by receptors on the RPE cell and ligands in the interphotoreceptor matrix bridging the RPE cell and phosphatidylserines at the POS surface, respectively.[16] Some receptors are common between phagocytosis and adhesion, but they use different ligands.[13–15,17] A loss of regulation of any of these important components of phagocytosis leads to vision loss in human disease and in rodent models.[13,18–20]

Here, we report results of studies of RPE phagocytosis and adhesion for the *Prpf3*$^{T494M/T494M}$, *Prpf8*$^{H2309P/H2309P}$, and *Prpf31*$^{+/-}$ mouse models. Specifically, we measured phagocytosis in primary RPE cultures from 2-week-old mice. Results indicate a deficiency in phagocytosis, which we also found in the human RPE cell line, ARPE-19, after shRNA-mediated knockdown of *PRPF31*. In addition, a loss of diurnal rhythmicity of phagocytosis and adhesion were detected *in vivo*. Interestingly, localization of key factors known to be involved in phagocytosis by RPE cells is modified. We conclude that the RPE is likely to be the primary site of pathogenesis in RNA splicing factor RP.

Materials and Methods

Animals

Animal research was performed under the protocols approved by the Institutional Animal Care and Use Committees at the Massachusetts Eye and Ear Infirmary and the Charles Darwin Animal Experimentation Ethics Committee from the Université Pierre et Marie Curie-Paris. An equal number of male and female mice were used in each of the following experiments.

Primary RPE Cell Culture

RPE cells from 9- to 10-day-old animals were isolated as described.[13] Briefly, eyecups were digested with 2 mg/mL hyaluronidase (Sigma-Aldrich, St. Louis, MO), and the neural retina was gently peeled from the eyecup. RPE was peeled from the Bruch's membrane after digestion with 1 mg/mL trypsin (Invitrogen, Carlsbad, CA) and seeded onto 5-mm glass coverslips. Cells were grown to confluence for 5 to 10 days in Dulbecco's modified Eagle's medium (DMEM) with 10% fetal bovine serum (FBS) at 37°C, 5% CO_2.

Primary Peritoneal Macrophage Cell Culture

Resident peritoneal macrophages were isolated as previously described.[21] Euthanized mice were pinned down to a dissection board, and the fur was dampened with 70% ethanol in a horizontal flow hood. The skin was delicately separated from the peritoneal wall by using forceps and scissors. Sterile phosphate-buffered saline (PBS; 5 mL) was injected into the abdominal cavity, and the belly was massaged or the whole body was shaken gently for 20 to 30 seconds. PBS was collected slowly from the cavity, and samples from two to three animals were pooled. Cells were spun for 10 minutes at 300 × *g* and resuspended in 1 mL of RPMI with 10% FBS. Cells were seeded in 96-well plates at 100,000 to 200,000 cells per well and allowed to adhere for 2 hours. Plates were shaken and wells were rinsed once with sterile PBS. Cells were maintained in medium for 2 to 3 days at 37°C, 5% CO_2.

Generation of Stable shRNA-*PRPF31* Knockdown ARPE-19 and J774.1 Cell Lines and Cell Viability Assay

Three shRNAs were designed to target human *PRPF31* or mouse *Prpf31* and cloned into pCAG-mir30 vector that contained a puromycin resistance gene. The sequences for these shRNAs are as follows: human shRNA1, 5′-TGCTGTTGACAGTGAGCGAGCAGATGAGCTCTTAGCTGATTAGTGAAGCCACAGATGTAATCAGCTAAGAGCTCATCTGCCTGCCTACTGCCTCGGA-3′; human shRNA2, 5′-TGCTGTTGACAGTGAGCGAACCCAACCTGTCCATCATTATTAGTGAAGCCACAGATGTAATAATGATGGACAGGTTGGGTGTGCCTACTGCCTCGGA-3′; and human shRNA3, 5′-TGCTGTTGACAGTGAGCGAGCTGAGTTCCTCAAGGTCAAGTAGTGAAGCCACAGATGTACTTGACCTTGAGGAACTCAGCCTGCCTACTGCCTCGGA-3′; mouse shRNA1, 5′-TGCTGTTGACAGTGAGCGCTCAGTCAAGAGCATTGCCAAGTAGTGAAGCCACAGATGTACTTGGCAATGCTCTTGACTGAATGCCTACTGCCTCGGA-3′; mouse shRNA2, 5′-TGCTGTTGACAGTGAGCGACCTGTCTGGCTTCTCTTCTACTAGTGAAGCCACAGATGTAGTAGAAGAGAAGCCAGACAGGGTGCCTACTGCCTCGGA-3′; and mouse shRNA3, 5′-TGCTGTTGACAGTGAGCGAGCCGAGTTCCTCAAGGTCAAGTAGTGAAGCCACAGATGTACTTGACCTTGAGGAACTCGGCCTGCCTACTGCCTCGGA-3′. We also cloned an

shRNA to green fluorescence protein into this vector as a nontargeted control (5′-TGCTGTTGACAGTGAGCGCTCTCCGAACGTGTATCACGTTTAGTGAAGCCACAGATGTAAACGTGATACACGTTCGGAGATTGCCTACTGCCTCGGA-3′). The shRNA-containing vectors were linearized with PstI and transfected into separate ARPE-19 (human RPE cell line; ATCC, Manassas, VA) or J774A.1 (mouse macrophage cell line; ATCC) cultures by using the Amaxa electroporation kit V (Amaxa Biosystems, Gaithersburg, MD). Transfected cells were transferred to six-well plates and 2 mL of culture medium (dilution 1:1 DMEM:F-12 with 10% FBS). Transfected cells were grown overnight at 37°C, 5% CO_2. Stable cell lines were selected with the addition of 1 (ARPE-19) to 1.25 (J774A.1) μg/mL puromycin (Sigma-Aldrich) 24 hours after transfection. Media and puromycin were refreshed every 2 days for 10 days. After selection, the four ARPE-19 and four J774A.1 knockdown lines were grown to confluence. To determine knockdown efficiency, stable lines were transiently transfected with either V5-tagged *PRPF31* in ARPE-19 cells or V5-tagged Prpf31 cloned in a Gateway Destination vector (Invitrogen). Western blot analysis was performed, and V5-tagged PRPF31 was quantified with an Odyssey Infrared Imager (LI-CORE Biosciences, Lincoln, NE). Cell viability assays were performed with the Cell Titer-Glo Luminescent Cell Viability Assay (Promega, Madison, WI) according to the manufacturer's recommendations. Briefly, ARPE-19 cells were seeded at a density of 1000 cells/well of a 96-well cell culture plate (catalog no. 3904; Corning, Corning, NY). Cells were grown for 3 days in DMEM with 10% FBS at 37°C, 5% CO_2. After this period, cell viability was measured by luminescence, and statistical significance was determined with the Student's *t*-test.

In Vitro Phagocytosis Assays

POSs were isolated from porcine eyes obtained fresh from the slaughterhouse and covalently labeled with fluorescein isothiocyanate (FITC) dye (Invitrogen) for *in vitro* phagocytosis assays as previously described.[13] Confluent cultured RPE cells were challenged with approximately 10 FITC-POSs per cell for 1.5 hours. Nonspecifically bound POSs were thoroughly removed with three washes in PBS with 1 mmol/L $MgCl_2$ and 0.2 mmol/L $CaCl_2$. To measure internalized POSs, some wells were incubated with trypan blue for 10 minutes to quench fluorescence of surface-bound FITC-labeled POSs as previously described.[22] Cells were fixed with ice-cold methanol, and nuclei were counterstained with Hoechst 33258 (Invitrogen) or DAPI (Euromedex, Strasbourg, France). Cells were imaged with a Nikon Ti2 (Nikon, Tokyo, Japan) or a Leica DM6000 (Leica, Wetzler, Germany) fluorescent microscope at ×20 magnification. For RPE primary cultures, FITC/DAPI ratios were calculated on all picture fields, corresponding to the number of POSs per cell. FITC-POSs were counted on a per cell basis for 100 cells, and the average was determined for three wells for ARPE-19. For peritoneal macrophages, FITC-POS and DAPI-labeled nuclei were quantified by fluorescence plate reading (Infinite M1000; Magellan version 6 software; Tecan, Durham, NC). Binding ratios were calculated by subtracting results obtained in internalization wells (trypan blue-treated) from total phagocytosis (untreated) wells. This was performed for three to six independent assays, and significance was determined with the Student's *t*-test ($P < 0.05$).

Before phagocytosis, confluent cultures of the stable knockdown J774A.1 lines were opsonized with Zymosan A Bioparticles Opsonizing Reagent (Life Technologies, Carlsbad, CA) according to the manufacturer's protocol. After opsonization, 1 μg of Zymosan A Bioparticles reconstituted in culture medium were applied to each culture well of a 96-well plate. The cultures were incubated at 37°C, 5% CO_2 for 1 hour. Fixation and determination of phagocytosis levels were performed as described above.

In Vivo Diurnal Rhythm Assays

Mice were euthanized at 2 hours before light onset (−2), at light onset (0), and 2, 4, and 8 hours (+2, +4, +8, respectively) after light onset, and processed for either electron microscopy or paraffin embedding as previously described.[13,15] For electron microscopy all reagents were purchased from Electron Microscopy Sciences (Hatfield, PA). Mice were perfused with 2% glutaraldehyde + 2% paraformaldehyde, and eyecups were transferred to perfusion buffer by adding 0.2 mol/L sodium cacodylate buffer. Ultrathin sections (60 to 80 nm) were stained with lead citrate/uranyl acetate, and early phagosomes were counted from 200 nm out from the optic nerve. An early phagosome was counted if it met the following criteria: it was contained within the cytoplasm of the RPE and had visible lamellar structure. For light microscopy, eyecups were fixed in formaldehyde/ethanol/acetic acid and embedded in paraffin by using Ottix Plus solvent substitute (DiaPath, Martinengo Berfamo, Italy). Five-micrometer sections were cut, and the paraffin was removed with SafeSolv solvent substitute. The sections were rehydrated and incubated in 5% H_2O_2 in 1× standard saline citrate for 10 minutes under illumination to bleach pigments. After blocking nonspecific signals by using 10% bovine serum albumin in 1× Tris-buffered saline, sections were stained with an anti-rhodopsin antibody (Millipore, Billerica, MA) and anti-mouse IgG-Alexa Fluor 488 (Invitrogen). Nuclei were stained with DAPI, and slides were mounted with Mowiol (prepared according to standard procedures). Image stacks were acquired on an Olympus FV1000 inverted confocal microscope (Olympus, Tokyo, Japan) with a 60× oil objective, a 4-time zoom, and 0.41-μm step size scans and were processed with the Photoshop CS6 software (Adobe Systems, Mountain View, CA). Areas of at least 100 μm of uninterrupted retina/RPE were counted on 10-scan stacks. In each experiment series, phagosome counts were normalized to length of retina and averaged. Significance was determined with the Student's *t*-test ($P < 0.05$) with two to five mice for all experiments.

In Vivo Retinal Adhesion Assays

We performed *in vivo* retinal adhesion assays as described.[14] Briefly, lens and cornea were removed from eyecups immediately after death in Hanks' saline buffer with calcium and magnesium. A radial cut was made to the optic nerve, and the neural retina was gently peeled from the flattened eyecup. Neural retina samples were lyzed in 50 mmol/L Tris-HCl (pH 7.5), 2 mmol/L EDTA, 150 mmol/L NaCl, 1% Triton X-100, 0.1% SDS, and 1% Nonidet P-40, with the addition of a protease inhibitors cocktail (Sigma-Aldrich) and 1 mmol/L phenylmethylsulfonyl fluoride. Proteins from cleared supernatants were quantified with the Bradford assay, and equal concentrations were immunoblotted for RPE65 (Abcam, Cambridge, MA, or Millipore) and β-actin (Abcam or Sigma-Aldrich). Melanin pigments were extracted from the insoluble neural retina pellet with 20% dimethyl sulfoxide, 2N NaOH. Samples and commercial melanin standards (Sigma-Aldrich) were quantified by measuring absorbance at 490 nm. Pigment abundance was normalized to protein concentration in each sample to account for different tissue yields. Bands from immunoblots were quantified with ImageJ version 1.46r (NIH, Bethesda, MD) by using a common sample on all blots as reference; signals were then averaged. Significance was determined with the Student's *t*-test ($P < 0.05$) with three to six neural retina samples for all experiments.

Immunofluorescence Microscopy

For cryosections, eyecups were fixed in 2% paraformaldehyde and incubated in 30% sucrose overnight at 4°C. Eyecups were embedded in optimum cutting temperature compound (Sakura, Finetek, Inc., Torrance, CA), and 10-μm sections were cut. Sections were individually incubated with primary antibodies against αv integrin (BD Biosciences, Franklin Lakes, NJ), β5 integrin (Santa Cruz Biotechnology, Santa Cruz, CA), MER proto-oncogene tyrosine kinase (MerTK; FabGennix, Frisco, TX), milk fat globule-EGF8 (Mfg-E8) and growth arrest-specific 6 (Gas6; R&D Systems, Minneapolis, MN), focal adhesion kinase (FAK) clone 2A7 (Millipore), and Protein S (Sigma-Aldrich), followed by IgG-Alexa Fluor 488 (Invitrogen). Nuclei were stained with DAPI and mounted with Fluoromount (Electron Microscopy Sciences). Images were taken with a Nikon Eclipse Ti inverted fluorescence microscope with an oil immersion 60× objective. Images were processed with NIS-Elements AR software version 3.22.14 (Nikon).

For paraffin sections, animals were sacrificed during the phagocytic peak, and eyes were fixed in Davidson fixative for 3 hours at 4°C, then lens and cornea were removed. Eyecups were embedded in paraffin, and 5-μm sections were cut. Sections were treated as described in In Vivo *Diurnal Rhythm Assays* and individually incubated with primary antibodies against αv integrin (Covance, Princeton, NJ); β5 integrin (Santa Cruz Biotechnology); Mfg-E8, MerTK, and Gas6 (R&D Systems); FAK clone 2A7 (Millipore); and Protein S (Novus Biologicals, Littleton, CO), followed by secondary antibody incubation with IgG-Alexa Fluor 488 (Invitrogen). Nuclei were stained with DAPI, and slides were mounted with Mowiol. Images were taken with a Leica DM6000 B Epi-fluorescence microscope with a 40× oil immersion objective. Images were processed with ImageJ version 1.46r and Photoshop CS6 (Adobe Systems) software.

Results

RPE Phagocytosis Is Decreased in *Prpf*-Mutant Mice

In the original characterization of the *Prpf*-mutant mice, electron microscopy identified morphological changes in the RPE of 1- to 2-year-old mutants.[8] Here, we wanted to determine whether functional changes precede the observed morphological changes. Because the RPE maintains phagocytic activity in culture, we established independent primary RPE cultures from 9- to 10-day-old $Prpf3^{T494M/T494M}$, $Prpf8^{H2309P/H2309P}$, $Prpf31^{+/-}$ mice and their corresponding littermate controls. Once the cultures were confluent, we used FITC-labeled porcine POSs and measured the phagocytosis after a 1.5-hour incubation. Images of primary cultures indicate the POS binding/uptake of RPE cells from the *Prpf*-mutant mice and their littermate controls and the qualitative deficiency in phagocytosis by the mutant mice (Figure 1A). In all three mutant models, 37% to 48% decrease in phagocytosis was observed ($n = 3$ to 5; $P < 0.05$) (Figure 1B). To account for nonspecific binding of POSs to the coverslips, we ran a negative control, in which the phagocytosis assay was performed on coverslips that did not contain cells. We observed no nonspecific adhesion of the POSs to the coverslips (data not shown).

We investigated if a specific step of phagocytosis between binding and internalization was preferentially perturbed in $Prpf31^{+/-}$ RPE primary cultures. After performing 1.5-hour phagocytic challenge, we treated the cells to quench the surface (bound POS) fluorescence to quantify solely internalized POSs. POS binding was significantly reduced by 53% ± 11% in mutant cells ($n = 2$ to 5; $P < 0.05$), whereas no significant difference was found in POS internalization rates between wild-type (WT) and mutant RPE cultures (Figure 1C).

Currently, 64 pathogenic mutations are known in *PRPF31*, of which many result in a frame shift and are degraded via the nonsense-mediated decay pathway.[2,10,11,23] ARPE-19 is a spontaneously immortalized human RPE cell line that is amenable to transfection and retains the ability to phagocytose.[24] To test whether mutations in the splicing factors also affect phagocytosis in a human RPE model, we generated three stable ARPE-19 cell lines with shRNA-mediated knockdown of *PRPF31* by using three distinct shRNAs directed against the 5′, 3′, and middle regions of the transcript (Figure 1D). We also generated a fourth stable cell line with an shRNA directed against the green fluorescent protein to use as a control. In each of the three PRPF31 shRNA stable cell lines we achieved approximately 60% to 95% knockdown of

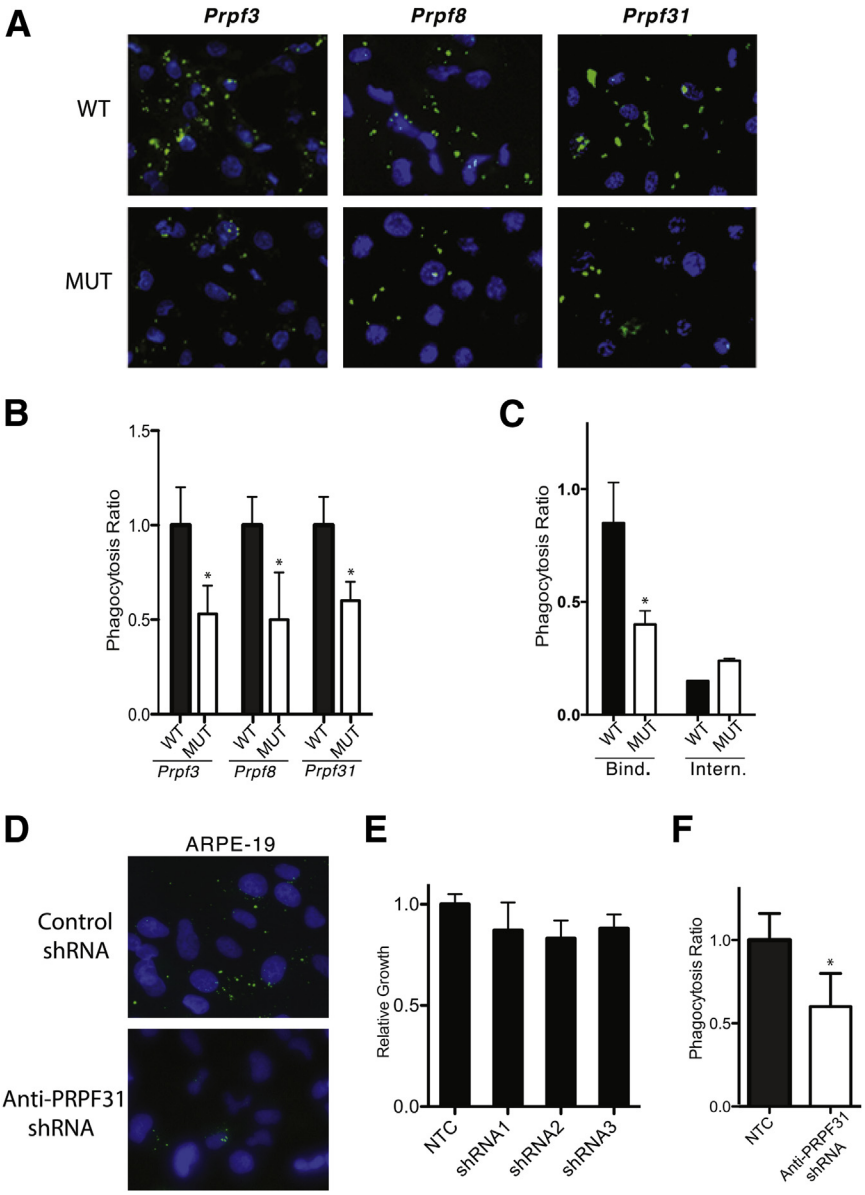

Figure 1 Inhibition of phagocytosis in *Prpf*-mutant mice. RPE primary cultures were established from 9- to 10-day-old *Prpf*-mutant mice and their littermate controls, then challenged with FITC-labeled porcine POSs and nuclei labeled with DAPI (blue). **A:** Qualitative representation of primary RPE cells from WT or $Prpf3^{T494M/T494M}$, $Prpf8^{H2309P/H2309P}$, $Prpf31^{+/-}$ MUT mice. A difference in POS uptake (green) was observed between the mutants and controls. **B:** Quantitative analysis of the phagocytic ratio showed a significant decrease in phagocytosis in the MUT mice compared with WT littermates for the three mutant mouse strains as indicated. **C:** Comparison of binding and internalization ratios of POSs between $Prpf31^{+/-}$ MUT mice and WT controls showed a significant decrease in Bind, but no significant change was seen in POS Intern in MUT mice. **D:** A stable line of shRNA-mediated knockdown of *PRPF31* in ARPE-19 cells. A difference in POS uptake (green) was observed between the control shRNA-transfected ARPE-19 cells and anti-PRPF31 shRNA-transfected ARPE-19 cells. **E:** Cell viability assay to determine the effect of *PRPF31*-knockdown in ARPE-19 cells showed no significant differences in cell growth or viability after shRNA-knockdown of *PRPF31* relative to the nontargeted control. **F:** shRNA-mediated knockdown of *PRPF31* in the human ARPE-19 cell line also significantly inhibited phagocytosis as shown by the decreased number of POSs per cell compared with NTCs. Data are expressed as means ± SD. $n = 3$ to 5 mice (**B**), $n = 2$ to 5 mice (**C**), $n = 6$ assays (**E**), $n = 3$ assays (**F**). $^*P < 0.05$. Bind, binding; Intern, internalization; MUT, mutant; NTC, nontargeting construct.

PRPF31 (data not shown). Cell viability assays of the shRNA-knockdown and nontargeted control ARPE-19 cells found that no significant decrease occurred in association with the knockdown of *PRPF31* (Figure 1E). Phagocytosis was decreased by approximately 40% in each line tested compared with the nontargeted control shRNA line (Figure 1F). As with the phagocytosis assay performed on primary RPE, we also performed a negative control assay and observed no nonspecific adhesion of the POSs to the coverslips (data not shown).

To determine whether disruption of the phagocytic machinery is an RPE-specific mechanism or can be observed in other phagocytic cells, we knocked down *Prpf31* in the mouse macrophage cell line, J774A.1. Similar to the knockdown studies in the ARPE-19 cell line, three distinct shRNAs were directed to the 5′- and 3′-termini and middle of the transcript. We used the same control shRNA as the previous studies. In each of the stable *Prpf31* cell lines, we achieved approximately 45% to 70% knockdown of *Prpf31* (Supplemental Figure S1A). We observed no phagocytosis deficiency in any of the lines tested (Supplemental Figure S1B). To ensure we did not observe nonspecific POS adhesion, we performed a negative control assay as for the previous experiment series (data not shown). Identical experiments were repeated on mouse primary peritoneal macrophages isolated from $Prpf31^{+/-}$ mice. Interestingly, neither step of phagocytosis, that is, binding or internalization, nor total phagocytosis was affected in *Prpf31*-mutant macrophages compared with WT macrophages (Supplemental Figure S1C).

Diurnal Rhythmicity of Phagocytosis Is Disrupted

Phagocytosis of shed POSs by the RPE followed a strong diurnal, synchronized rhythm, peaking at 2 hours after light onset and remaining relatively inactive for the remainder of the

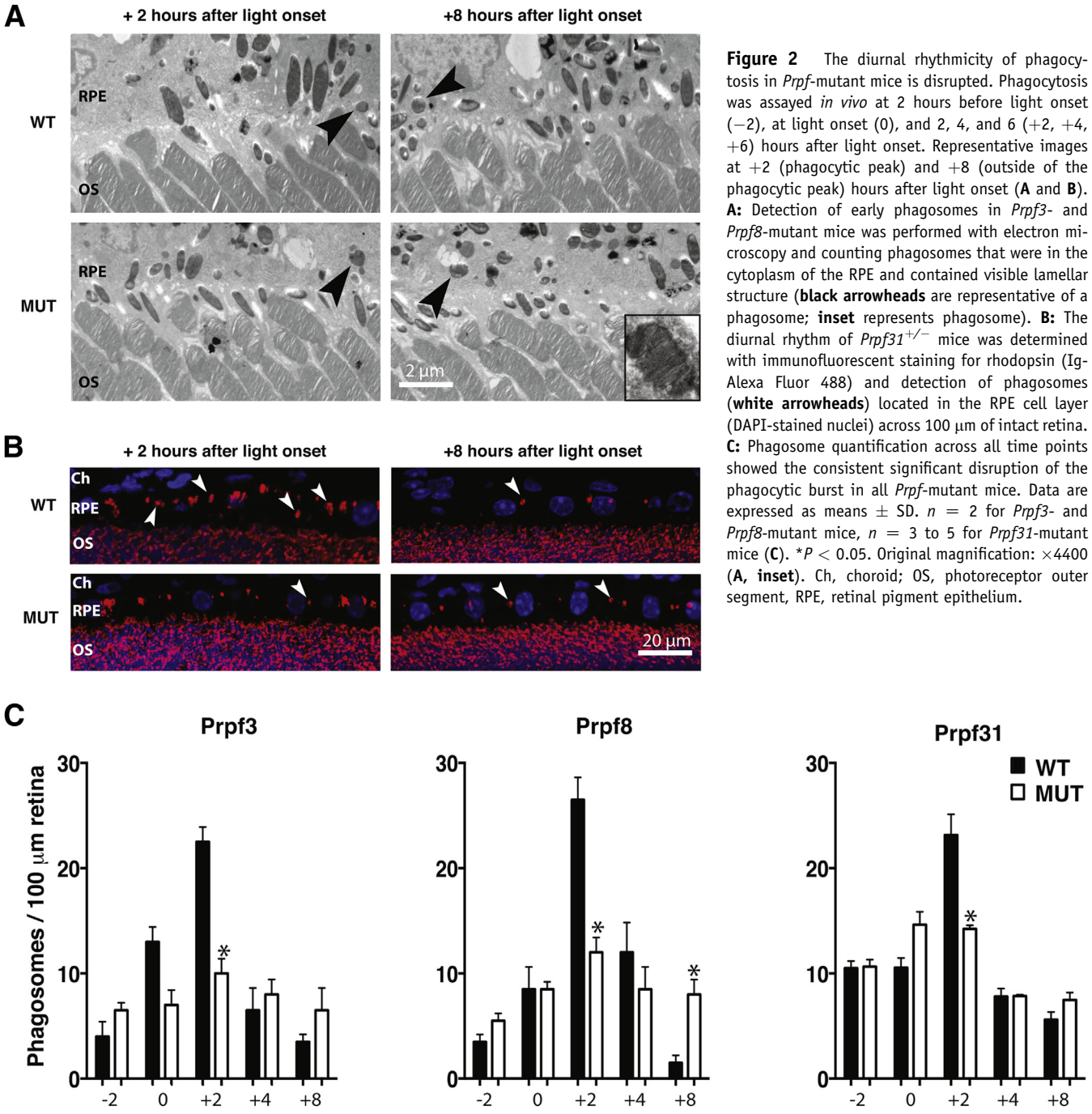

Figure 2 The diurnal rhythmicity of phagocytosis in *Prpf*-mutant mice is disrupted. Phagocytosis was assayed *in vivo* at 2 hours before light onset (−2), at light onset (0), and 2, 4, and 6 (+2, +4, +6) hours after light onset. Representative images at +2 (phagocytic peak) and +8 (outside of the phagocytic peak) hours after light onset (**A** and **B**). **A:** Detection of early phagosomes in *Prpf3*- and *Prpf8*-mutant mice was performed with electron microscopy and counting phagosomes that were in the cytoplasm of the RPE and contained visible lamellar structure (**black arrowheads** are representative of a phagosome; **inset** represents phagosome). **B:** The diurnal rhythm of *Prpf31*$^{+/-}$ mice was determined with immunofluorescent staining for rhodopsin (IgAlexa Fluor 488) and detection of phagosomes (**white arrowheads**) located in the RPE cell layer (DAPI-stained nuclei) across 100 μm of intact retina. **C:** Phagosome quantification across all time points showed the consistent significant disruption of the phagocytic burst in all *Prpf*-mutant mice. Data are expressed as means ± SD. $n = 2$ for *Prpf3*- and *Prpf8*-mutant mice, $n = 3$ to 5 for *Prpf31*-mutant mice (**C**). $^*P < 0.05$. Original magnification: ×4400 (**A, inset**). Ch, choroid; OS, photoreceptor outer segment, RPE, retinal pigment epithelium.

day.[13] We measured phagocytosis *in vivo* at 5 time points throughout the light cycle by using either electron microscopy (Figure 2A) or immunofluorescence (Figure 2B), both recognized techniques to assess the RPE phagocytic rhythm.[13,15] For *Prpf3* and *Prpf8* control and mutant mice we counted early phagosomes that contained lamellar structures on electron micrographs (Figure 2A). Phagocytosis rhythmicity was determined in *Prpf31*$^{+/-}$ mice by using paraffin embedding and staining for rhodopsin, and we counted phagosomes present in the RPE cell layer (Figure 2B). We observed a phagocytosis burst at 2 hours after light onset in all control mice, identifying 22 to 26 phagosomes per 100 μm of retinal section (Figure 2C). In contrast, mutant mice only displayed 10 to 14 phagosomes at the same peak time point. During the rest of the light/dark cycle, phagocytosis levels remained relatively low in control mice (off-peak hours, 2 to 12 phagosomes/100 μm retina), and these levels were increased in mutant mice (6 to 14 phagosomes/100 μm retina). These results indicated a decrease in the phagocytic peak intensity in all three types of mutant mice, with a spreading of the time of the peak that lasted longer in *Prpf3* and *Prpf8* mutants and started earlier in *Prpf31* mutants. Further, the *Prpf8* mutants have

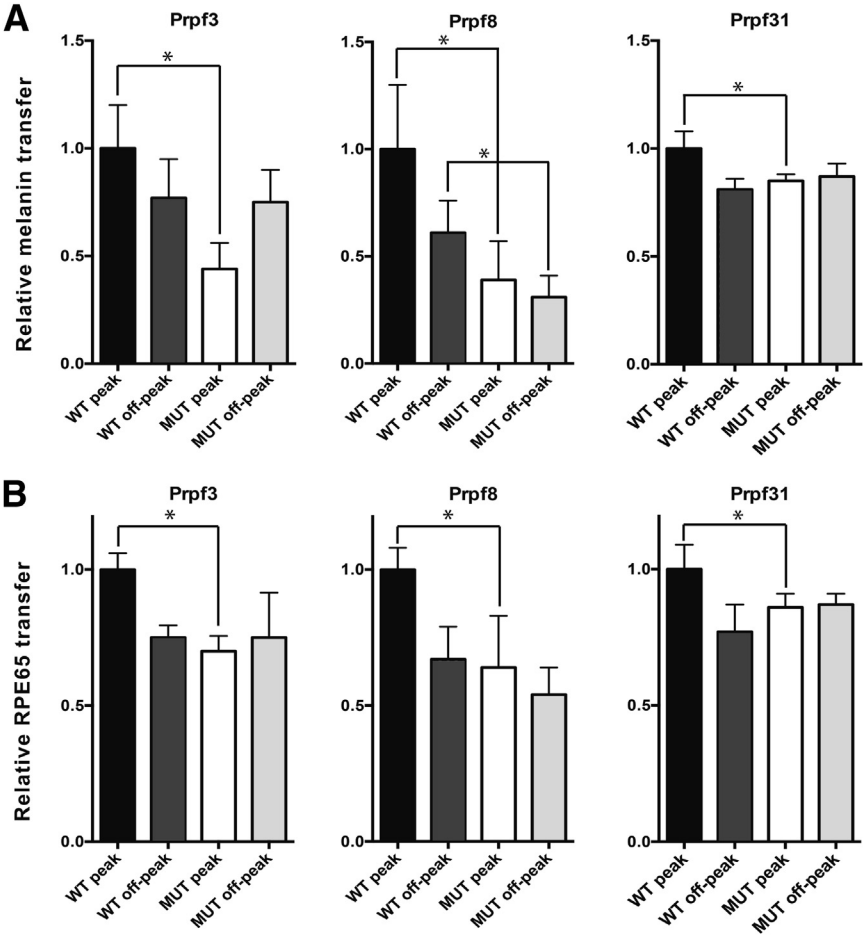

Figure 3 Alterations in retinal adhesion in *Prpf*-mutant mice at the peak time point. Adhesive strength between RPE apical microvilli and POSs was determined by quantifying the amount of RPE pigments or proteins that adheres to the neural retina, relative to the WT control. **A:** Melanin quantification showed that adhesion was decreased in all three mutant mice strains at the peak time point 3.5 hours after light onset and in $Prpf8^{H2309P/H2309P}$ mice at the off-peak time point. **B:** Quantitative measurements of RPE65 proteins on immunoblots confirm the melanin findings in all three mutant mice strains at the peak time point; however, only a trend was observed for decrease in adhesion at the off-peak time point in *Prpf8*-mutant mice. Data are expressed as means ± SD. $n = 3$ to 7 mice (**A**), $n = 4$ to 7 mice (**B**). $^*P < 0.05$.

more phagosomes at the off-peak time point (8 hours), relative to the WT controls.

Decreased Retinal Adhesion Is Observed at the Peak Time Point

Adhesion between the RPE apical microvilli and distal tips of the POSs followed a synchronized rhythm with maximum strength occurring 3.5 hours after light onset, slightly after the phagocytic peak.[14,15] Adhesion could be determined by peeling the retina from a flattened eyecup immediately after euthanasia, then quantifying both the RPE melanin content and apical RPE protein markers, such as RPE65, transferred to the retina. With the use of this method, we assessed adhesion in *Prpf*-mutant mice and littermate controls at 3.5 and 8.5 hours after light onset (peak and off-peak adhesion, respectively). RPE adhesion was quantified first by using a standard melanin quantification procedure,[14] then Western blot analysis for the presence of RPE65 to confirm the melanin results. We noted a decrease of 56% ± 16% ($n = 6$; $P < 0.05$; variation is equal to the SD) of the melanin content in the $Prpf3^{T494M/T494M}$ mice at peak time and no significant change in adhesion at the off-peak time point (Figure 3A). Western blot analysis confirmed this observation with a 30% ± 2% decrease in peak adhesion (Figure 3B). Melanin quantification in $Prpf8^{H2309P/H2309P}$ mice found that adhesion was significantly decreased by 61% ± 28% at the peak time point and 51% ± 16% at the off-peak time point ($n = 6$; $P < 0.05$ for both time points) (Figure 3A). Western blot analysis, however, confirmed a significant 36% ± 11% decrease only at the peak time point (Figure 3B). In the $Prpf31^{+/-}$ mice, a 15% ± 1% decrease was observed at the peak time point (Figure 3A) and was confirmed by immunoblot analysis (14% ± 1%; $n = 3$ to 7; $P < 0.05$ for both panels) (Figure 3B).

Localization of Phagocytosis and Adhesion Markers

RPE cells are highly polarized, and their function depends on this polarity.[25] The specific localization of many proteins expressed in the RPE is important, and irregularities in localization may cause retinal dystrophies such as RP or Best disease.[26,27] Given the disruption of the diurnal rhythm of both phagocytosis and adhesion in all three *Prpf*-mutant mouse models, we wanted to characterize the localization of the proteins that are known to be important for these processes. Protein localization was assayed on cryosections for *Prpf3*- and *Prpf8*-mutant mice (Figure 4) and on paraffin sections for *Prpf31*-mutant mice (Figure 5).

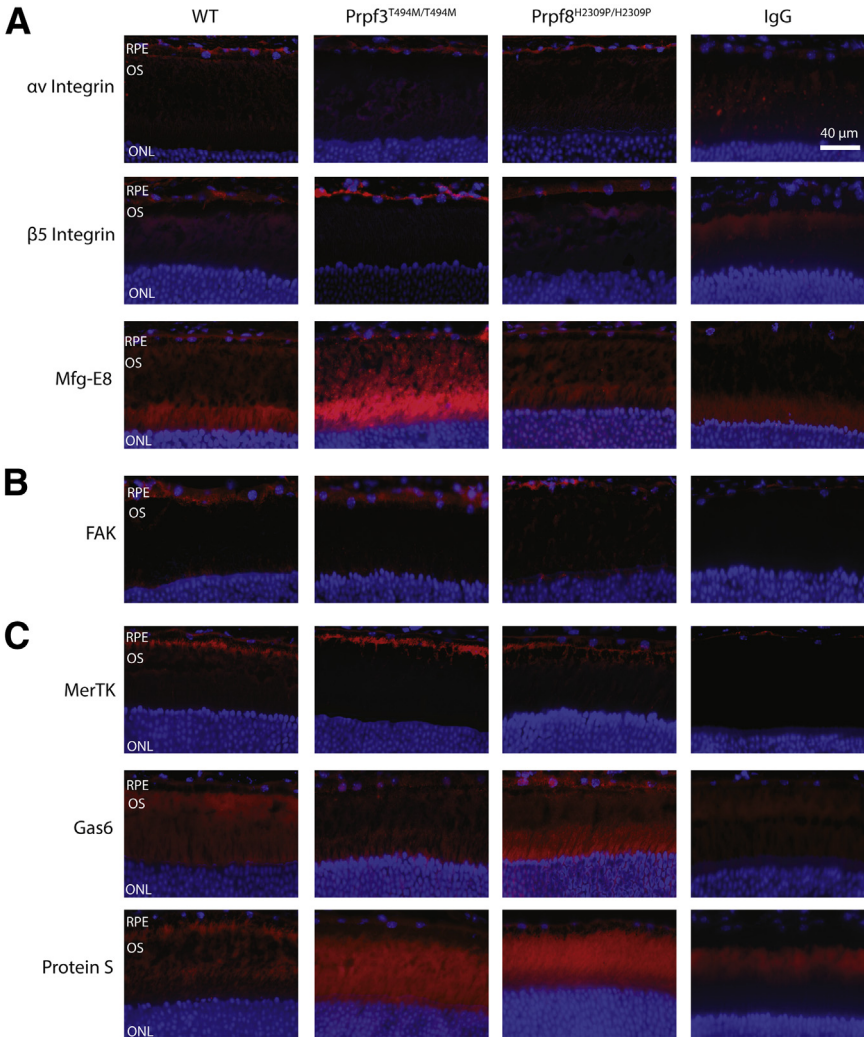

Figure 4 Localization and expression of some adhesion and phagocytosis markers are perturbed in *Prpf3*- and *Prpf8*-mutant mice. Representative images of the expression and localization of αv and β5 integrin receptor subunits and associated Mfg-E8 ligand (**A**), FAK intracellular signaling protein (**B**), and MerTK receptors and associated Gas6 and Protein S ligands (**C**) on WT control as well as *Prpf3*- and *Prpf8*-mutant retinal cryosections as indicated. Images from sections probed with nonimmune IgG (IgG) are included for each antigen. Localization of β5 integrin to the basal side of the RPE was observed in both *Prpf3*- and *Prpf8*-mutant mice. In addition, FAK was mislocalized in *Prpf8*-mutant mice to the basal side of the RPE. Each protein of interest was stained with Ig-Alexa Fluor 488, and nuclei were stained with DAPI. ONL, outer nuclear layer; OS, photoreceptor outer segments, RPE, retinal pigment epithelium.

As reported previously, the main phagocytic receptors (αvβ5 integrin and MerTK) localized at the RPE apical surface,[22] whereas their ligands were expressed throughout the POS and RPE.[28] Interestingly, extracellular ligands expressed in the interphotoreceptor matrix can be synthesized by both RPE and photoreceptor cells.

It was reported that αvβ5-integrin with its associated ligand Mfg-E8 are important for phagocytosis and are responsible for the diurnal rhythmicity of this function.[13,15] In addition, αvβ5-integrin participates in retinal adhesion and its rhythm, but with a ligand different from Mfg-E8.[14,15,17] αv Integrin subunits associate in complexes with several β integrin subunits in RPE cells[14]; therefore, it was more relevant to analyze the expression of β5 integrin subunits. Thus, we probed for the αv and β5 subunits of the αvβ5 integrin receptor separately. In WT tissues each integrin localized primarily to the apical side of the RPE, with some expression throughout the RPE cells. In all three *Prpf*-mutant tissues, no change was observed in αv-integrin localization (Figures 4A and 5A). In contrast, β5 integrin localized primarily to the basal side of the RPE in the *Prpf3*- and *Prpf31*-mutant tissues, whereas it displayed expression equally throughout the RPE in *Prpf8*-mutant RPE cells. We observed no change in the localization of Mfg-E8 in either the RPE or POS.

The downstream signaling protein FAK provided a sequential activation link between αvβ5 integrin and MerTK receptors both *in vitro* and *in vivo*.[13,29,30] FAK was found throughout the RPE, and no change to this pattern was observed in the *Prpf3*- or the *Prpf31*-mutant mice (Figures 4B and 5B). *Prpf8*-mutant mice, however, showed FAK localization to the basal side of the RPE.

Phagocytosis is driven by the timely activation of MerTK via phosphorylation at the time of the activity peak.[13,15,31] Gas6 and Protein S are ligands of MerTK that can stimulate uptake of shed outer segments *in vitro*.[32] Both ligands are necessary to the internalization of POS because double knockout animals recapitulate the rapid retinal degeneration that occurs in rats in whose MerTK receptors are absent.[33] MerTK expression in WT tissues was localized to both the apical and basal membranes of the RPE, whereas MerTK was localized solely to the apical side of *Prpf31*-mutant RPE cells (Figures 4C and 5C). The first

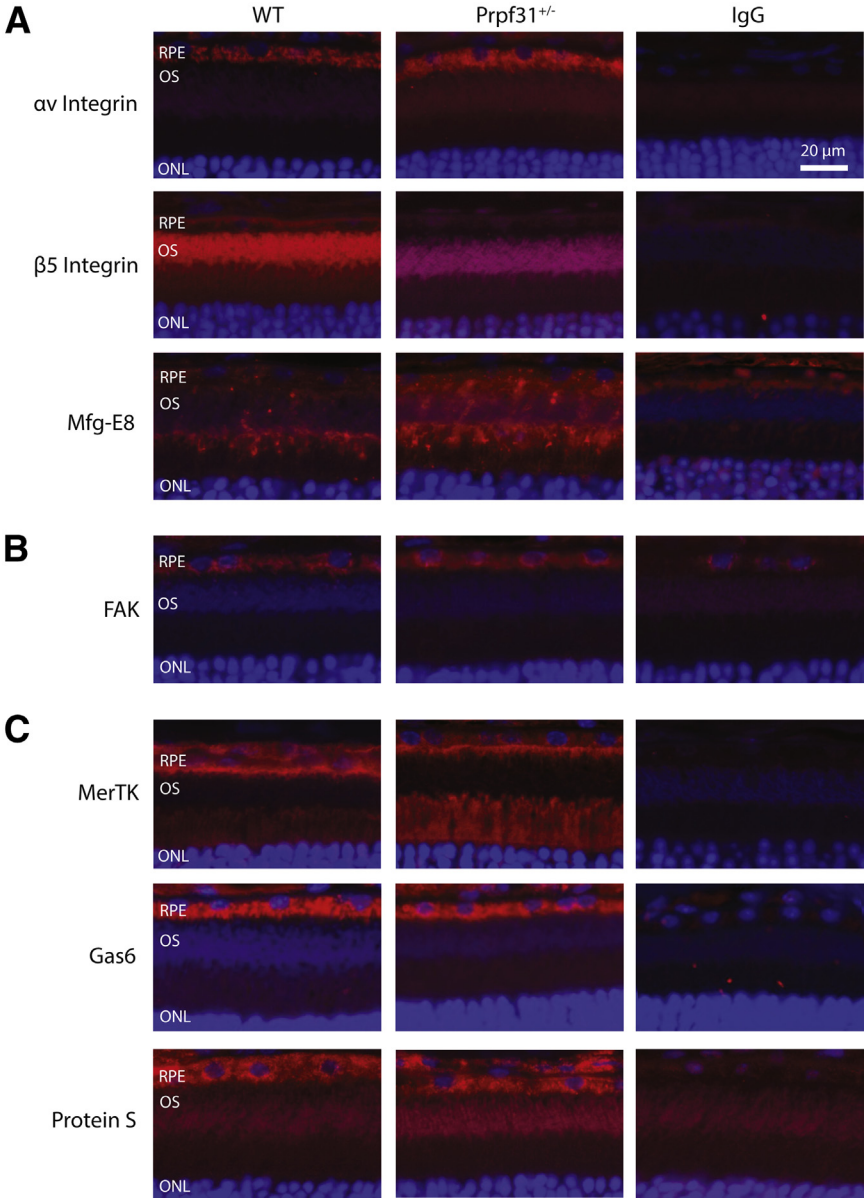

Figure 5 Localization and expression of some adhesion and phagocytosis markers are perturbed in *Prpf31*-mutant mice. Representative images of the expression and localization of αv and β5 integrin receptor subunits and associated Mfg-E8 ligand (**A**), FAK intracellular signaling protein (**B**), and MerTK receptors and associated Gas6 and Protein S ligands (**C**) or nonimmune IgG (IgG) on WT control and *Prpf31*-mutant retinal paraffin sections as indicated. The most notable change in *Prpf31*-mutant mice was the mislocalization of β5 integrin to the basal side of the RPE, whereas localization of MerTK was also perturbed. Each protein of interest was stained with IgG-Alexa Fluor 488, and nuclei were stained with DAPI. ONL, outer nuclear layer; OS, photoreceptor outer segments, RPE, retinal pigment epithelium.

MerTK ligand Gas6 localized to the POS and apical layer of the RPE in WT tissues. Diffuse expression was seen throughout the RPE of *Prpf3*-mutant mice. *Prpf8*-mutant mice maintained Gas6 expression in the POS but appeared to lose apical localization in the RPE, also indicating a diffuse expression throughout the RPE. No localization changes could be observed in *Prpf31*-mutant mice. The expression of the second MerTK ligand Protein S was localized specifically to the POS in WT and all *Prpf*-mutant mice (Figures 4C and 5C).

Discussion

The molecular mechanism by which mutations in the five RNA splicing factor genes associated with RP cause disease has yet to be determined. A first step toward understanding the pathogenesis of RNA splicing factor RP is the identification of which of the >60 cell types in the retina is primarily affected by mutations in the RNA splicing factors.[34,35] Although these findings must be confirmed in patients with RNA splicing factor RP, generation of the *Prpf3*-T494M, *Prpf8*-H2309P, and *Prpf31*$^{+/-}$ mouse models provided, for the first time, insight into the specific cell type affected by mutations in these genes.[8] Morphological changes in the RPE suggested that the RPE, and not the neural retina, was the primary site of pathogenesis. In this study, we investigated the RPE phenotype in more detail and found that phagocytosis and retinal adhesion, two critical RPE functions for the retina, are impaired from an early age. We found that adhesion between the apical RPE microvilli and POSs and phagocytosis of normal spent POSs are both decreased. In addition, the diurnal rhythmicity of these two functions is

disturbed. We observed changes to the localization of some of the major receptors and ligands that facilitate these processes. These findings provide strong evidence that the RPE is likely to be the primary cell affected by mutations in the RNA splicing factors in the mouse.

One of the main functions that the RPE performs is the rhythmic binding and internalization of shed POSs daily.[12] To complete phagocytosis, the apical microvilli of the RPE specifically recognize the POS via αvβ5 integrin receptor binding to its ligand Mfg-E8.[13,15] Timely POS recognition by αvβ5 integrin receptors initiates a signaling cascade, leading to phosphorylation of MerTK, which is responsible for internalization of the bound particles.[13,36] In the primary RPE cultures of the *Prpf* mutant mice, we found a significant decrease in phagocytosis. Because these studies were performed with isolated RPE cells and normal POSs pooled from several porcine eyes, the results indicate that the decreased phagocytosis observed in the mutant cells is due to a cell autonomous process. In *Prpf31*-mutant mice the binding of POS, rather than internalization, was decreased. Binding and internalization are functionally distinct, suggesting that binding of POS is the primary function disrupted in this model.[13] Because these assays were performed with cells from young animals, these results suggest that mutations in the RNA splicing factors cause alterations in RPE function at an early age and are intrinsically present in RPE cells. Therefore, the phenotype appearing in aging animals also suggests that degeneration is possibly the result of a cumulative process.

Haploinsufficiency is likely the cause of dominant disease with mutations in *PRPF31*, and this provides an opportunity to develop a knockdown model of disease in the human ARPE-19 cell line.[2,10] With the use of shRNAs directed against *PRPF31*, we generated three stable knockdown lines in ARPE-19 cells. The phagocytosis assays were performed in the same manner as in the primary mouse culture system, and a similar deficiency in phagocytosis was observed. This not only adds to the evidence that haploinsufficiency is the mechanism of disease in cases of *PRPF31* mutations but also suggests that the functional mechanism observed in mice is likely to apply to affected humans.

RNA splicing RP is characterized as a nonsyndromic disease, and this allows us to study whether defects in phagocytosis of the RPE are caused by RPE-specific mechanisms or generalized defects in common phagocytic processes. We knocked down *Prpf31* in the mouse macrophage cell line, J774A.1, tested peritoneal macrophages from the *Prpf31*-mutant mice, and observed no loss of phagocytic function. This finding suggests that general macrophage function is not affected, and RPE-specific phagocytic mechanisms appear to be the cause of the deficiency. Further, patients with RNA splicing factor RP do not present with any macrophage-associated disease, adding additional evidence in support of an RPE-specific deficiency.

Knockout mouse models of β5 integrin have found the importance of αvβ5 integrin receptors for both RPE phagocytosis and retinal adhesion.[13,14] Peak phagocytosis occurs before peak adhesion 2 hours after light onset, and a loss of this synchronicity leads to retinal dysfunction with age.[13] In the *Prpf*-mutant models, we used two independent techniques, electron microscopy in *Prpf3* and *Prpf8* models and immunofluorescence in the *Prpf31* model, to study the phagocytic diurnal rhythm, both techniques previously validated as giving comparable results.[13,15] We found that peak phagocytosis, in all cases, was reduced at 2 hours after light onset, with a peak activity appearing attenuated and more widespread in time. Peak adhesion occurs at 3.5 hours after light onset, after a similar synchronous rhythm occurring just after peak phagocytosis.[14] In each of the *Prpf*-mutant mouse models studied, we found that adhesion was significantly decreased at the peak time point, down to levels detected at the off-peak time. These data suggest that functional deficiencies in both phagocytosis and adhesion in the RPE are a result of these mutations and may contribute to the pathogenesis of disease. Interestingly, the peak activity time of both functions is perturbed *in vivo*, whereas phagocytosis and adhesion seem relatively normal at other times. These results suggest that cyclic activities may be affected and need to be studied in more detail.

The coordination of the phagocytic diurnal rhythm is reliant on many factors, including the expression of the proper receptors, the polarity of the RPE, the expressed ligands, and signaling pathways.[12] Mfg-E8 has been identified as an extracellular ligand that is required for maintaining the phagocytic but not the adhesive synchronicity of the RPE.[13,15] The RPE in mice lacking either β5 integrin receptors or Mfg-E8 ligands do not experience a phagocytic peak; however, the neural retina does not degenerate in any of these two models even if vision loss occurs in β5 knockout mice.[13] The *Prpf*-mutant mice display a similar phenomenon, suggesting that the retina is tolerant of a dysfunctional RPE, at least for a period of time. But unlike β5 integrin- and Mfg-E8−deficient mice, it is unknown which factors are responsible for the phagocytosis and adhesion deficiencies in the *Prpf*-mutant mice; therefore, we decided to interrogate the known phagocytosis-related receptors and ligands.

Immunofluorescence analyses of the localization of the primary RPE phagocytosis ligands and receptors in the RPE and POSs found mislocalization of β5-integrin in all three mutant mouse models and FAK in *Prpf8*-mutant mice. Aberrant splicing resulting in direct protein mislocalization has been implicated in diseases such as Fukuyama muscular dystrophy.[37] Alternatively, mislocalization could be the result of aberrant splicing of secondary factors such as components required for protein trafficking.[38] It is unknown if the extent of dysfunction observed in our study can be the result of the mislocalized receptors and ligands. Various methods are available to examine if aberrantly spliced transcripts are produced in RPE cells, such as reverse

transcription PCR of full-length transcripts, or of specific gene portions, and Northern blot analysis. However, they all present major flaws because aberrant transcripts might not be detected because of primer or probe design or because of the lack of information on which exons would be targeted by the missplicing. Currently, the most effective method for detecting aberrant transcripts is the use of RNA-Seq analyses. Indeed, RNA-Seq allowed us to discover thousands of alternative terminal exons in the human retinal transcriptome.[39] We have established models that permit us to perform these much broader studies of RNA splicing in these forms of RP, although those experiments are beyond the scope of the present study.

Here, we report the first functional characterization of the RPE in mice with mutations in the RNA splicing factors *Prpf3*, *Prpf8*, and *Prpf31*. As we have previously reported, the mutant mice do not experience photoreceptor degeneration but rather morphological changes in the RPE.[8] Because RNA splicing factor RP is a late-onset disease, these results are not surprising, and the models afford us the ability to study the mechanisms leading to the onset of disease. Our results indicate that the RPE is likely to be the primary cell type affected by mutations in these three RNA splicing factors in the mouse and in humans, given the similar phagocytic deficiency observed in *PRPF31*-knockdown human ARPE-19 cells. Although the exact mechanism of disease pathogenesis remains to be identified, these data will allow for future research to be focused on the RPE. For example, the identification of the RPE as the primary cell type affected in these disorders will make it possible to extend these studies to human cells, because it is now possible to generate RPE cells from human induced pluripotent stem cells of patients with inherited retinal diseases.[40–42] One of the most vital questions that remains to be answered is whether mutations in these splicing factors specifically alter the proteins that are required for proper adhesion and phagocytosis of shed POSs. Because it appears that splicing of the mRNAs for the main phagocytosis receptors and ligands is not altered in the *Prpf*-mutant mice, perhaps secondary factors are disrupted, such as signaling pathways or circadian regulation of cellular functions or gene expression in general. The neural retina and RPE function integrally, so it is possible that a process important for adhesion and phagocytosis is disrupted in the neural retina as well.[13,14] With the era of retinal gene therapy, it will be important to fully answer these questions so that effective therapies can be designed for the RNA splicing factor forms of RP.

Acknowledgments

We thank Stéphane Fouquet (Imaging Facility, Institut de la Vision, Moreau, Paris) for help with confocal microscopy, Marie-Laure Niepon (Histology Facility, Institut de la Vision, Moreau, Paris) for treatment of paraffin samples, and Bertrand Calippe for help with peritoneal macrophages isolation.

Supplemental Data

Supplemental material for this article can be found at *http://dx.doi.org/10.1016/j.ajpath.2014.06.026*.

References

1. Will CL, Luhrmann R: Spliceosome structure and function. Cold Spring Harb Perspect Biol 2011, 3
2. Liu MM, Zack DJ: Alternative splicing and retinal degeneration. Clin Genet 2013, 84:142–149
3. Daiger SP, Bowne SJ, Sullivan LS: Perspective on genes and mutations causing retinitis pigmentosa. Arch Ophthalmol 2007, 125:151–158
4. Hartong DT, Berson EL, Dryja TP: Retinitis pigmentosa. Lancet 2006, 368:1795–1809
5. Sullivan LS, Bowne SJ, Reeves MJ, Blain D, Goetz K, Ndifor V, Vitez S, Wang X, Tumminia SJ, Daiger SP: Prevalence of mutations in eyeGENE probands with a diagnosis of autosomal dominant retinitis pigmentosa. Invest Ophthalmol Vis Sci 2013, 54:6255–6261
6. Nishiguchi KM, Rivolta C: Genes associated with retinitis pigmentosa and allied diseases are frequently mutated in the general population. PLoS One 2012, 7:e41902
7. Neveling K, Collin RW, Gilissen C, van Huet RA, Visser L, Kwint MP, Gijsen SJ, Zonneveld MN, Wieskamp N, de Ligt J, Siemiatkowska AM, Hoefsloot LH, Buckley MF, Kellner U, Branham KE, den Hollander AI, Hoischen A, Hoyng C, Klevering BJ, van den Born LI, Veltman JA, Cremers FPM, Scheffer H: Next-generation genetic testing for retinitis pigmentosa. Hum Mutat 2012, 33:963–972
8. Graziotto JJ, Farkas MH, Bujakowska K, Deramaudt BM, Zhang Q, Nandrot EF, Inglehearn CF, Bhattacharya SS, Pierce EA: Three gene-targeted mouse models of RNA splicing factor RP show late-onset RPE and retinal degeneration. Invest Ophthalmol Vis Sci 2011, 52: 190–198
9. Graziotto JJ, Inglehearn CF, Pack MA, Pierce EA: Decreased levels of the RNA splicing factor Prpf3 in mice and zebrafish do not cause photoreceptor degeneration. Invest Ophthalmol Vis Sci 2008, 49:3830–3838
10. Rio Frio T, Wade NM, Ransijn A, Berson EL, Beckmann JS, Rivolta C: Premature termination codons in PRPF31 cause retinitis pigmentosa via haploinsufficiency due to nonsense-mediated mRNA decay. J Clin Invest 2008, 118:1519–1531
11. Venturini G, Rose AM, Shah AZ, Bhattacharya SS, Rivolta C: CNOT3 is a modifier of PRPF31 mutations in retinitis pigmentosa with incomplete penetrance. PLoS Genet 2012, 8:e1003040
12. Kevany BM, Palczewski K: Phagocytosis of retinal rod and cone photoreceptors. Physiology (Bethesda) 2010, 25:8–15
13. Nandrot EF, Kim Y, Brodie SE, Huang X, Sheppard D, Finnemann SC: Loss of synchronized retinal phagocytosis and age-related blindness in mice lacking alphavbeta5 integrin. J Exp Med 2004, 200:1539–1545
14. Nandrot EF, Anand M, Sircar M, Finnemann SC: Novel role for alphavbeta5-integrin in retinal adhesion and its diurnal peak. Am J Physiol Cell Physiol 2006, 290:C1256–C1262
15. Nandrot EF, Anand M, Almeida D, Atabai K, Sheppard D, Finnemann SC: Essential role for MFG-E8 as ligand for alphavbeta5 integrin in diurnal retinal phagocytosis. Proc Natl Acad Sci U S A 2007, 104:12005–12010
16. Ruggiero L, Connor MP, Chen J, Langen R, Finnemann SC: Diurnal, localized exposure of phosphatidylserine by rod outer segment tips in wild-type but not Itgb5-/- or Mfge8-/- mouse retina. Proc Natl Acad Sci U S A 2012, 109:8145–8148
17. Nandrot EF, Finnemann SC: Lack of alphavbeta5 integrin receptor or its ligand MFG-E8: distinct effects on retinal function. Ophthalmic Res 2008, 40:120–123
18. Nandrot E, Dufour EM, Provost AC, Péquignot MO, Bonnel S, Gogat K, Marchant D, Rouillac C, Sépulchre de Condé B, Bihoreau MT, Shaver C,

Dufier JL, Marsac C, Lathrop M, Menasche M, Abitbol MM: Homozygous deletion in the coding sequence of the c-mer gene in RCS rats unravels general mechanisms of physiological cell adhesion and apoptosis. Neurobiol Dis 2000, 7:586–599
19. Gal A, Li Y, Thompson DA, Weir J, Orth U, Jacobson SG, Apfelstedt-Sylla E, Vollrath D: Mutations in MERTK, the human orthologue of the RCS rat retinal dystrophy gene, cause retinitis pigmentosa. Nat Genet 2000, 26:270–271
20. Tschernutter M, Jenkins S, Waseem N, Saihan Z, Holder G, Bird A, Bhattacharya S, Ali R, Webster A: Clinical characterisation of a family with retinal dystrophy caused by mutation in the Mertk gene. British J Ophthalmol 2006, 90:718–723
21. Davies JQ, Gordon S: Isolation and culture of murine macrophages. Methods Mol Biol 2005, 290:91–103
22. Finnemann SC, Bonilha VL, Marmorstein AD, Rodriguez-Boulan E: Phagocytosis of rod outer segments by retinal pigment epithelial cells requires αvβ5 integrin for binding but not for internalization. Proc Natl Acad Sci U S A 1997, 94:12932–12937
23. Stenson PD, Mort M, Ball EV, Shaw K, Phillips AD, Cooper DN: The Human Gene Mutation Database: building a comprehensive mutation repository for clinical and molecular genetics, diagnostic testing and personalized genomic medicine. Hum Genet 2014, 133:1–9
24. Mao Y, Finnemann S: Analysis of photoreceptor outer segment phagocytosis by RPE cells in culture. Retinal Degeneration. Edited by Weber BH, Langmann T. Humana Press, 2013. pp. 285–295
25. Marmorstein AD: The polarity of the retinal pigment epithelium. Traffic 2001, 2:867–872
26. Davidson AE, Millar ID, Urquhart JE, Burgess-Mullan R, Shweikh Y, Parry N, O'Sullivan J, Maher GJ, McKibbin M, Downes SM, Lotery AJ, Jacobson SG, Brown PD, Black GC, Manson FD: Missense mutations in a retinal pigment epithelium protein, bestrophin-1, cause retinitis pigmentosa. Am J Hum Genet 2009, 85:581–592
27. Lopes VS, Gibbs D, Libby RT, Aleman TS, Welch DL, Lillo C, Jacobson SG, Radu RA, Steel KP, Williams DS: The Usher 1B protein, MYO7A, is required for normal localization and function of the visual retinoid cycle enzyme, RPE65. Hum Mol Genet 2011, 20:2560–2570
28. Prasad D, Rothlin CV, Burrola P, Burstyn-Cohen T, Lu Q, Garcia de Frutos P, Lemke G: TAM receptor function in the retinal pigment epithelium. Mol Cell Neurosci 2006, 33:96–108
29. Finnemann SC: Focal adhesion kinase signaling promotes phagocytosis of integrin-bound photoreceptors. EMBO J 2003, 22:4143–4154
30. Qin S, Rodrigues GA: Roles of alphavbeta5, FAK and MerTK in oxidative stress inhibition of RPE cell phagocytosis. Exp Eye Res 2012, 94:63–70
31. Nandrot EF, Silva KE, Scelfo C, Finnemann SC: Retinal pigment epithelial cells use a MerTK-dependent mechanism to limit the phagocytic particle binding activity of alphavbeta5 integrin. Biol Cell 2012, 104:326–341
32. Hall MO, Obin MS, Heeb MJ, Burgess BL, Abrams TA: Both protein S and Gas6 stimulate outer segment phagocytosis by cultured rat retinal pigment epithelial cells. Exp Eye Res 2005, 81:581–591
33. Burstyn-Cohen T, Lew ED, Través PG, Burrola PG, Hash JC, Lemke G: Genetic dissection of TAM receptor-ligand interaction in retinal pigment epithelial cell phagocytosis. Neuron 2012, 76:1123–1132
34. Yin J, Brocher J, Fischer U, Winkler C: Mutant Prpf31 causes pre-mRNA splicing defects and rod photoreceptor cell degeneration in a zebrafish model for retinitis pigmentosa. Mol Neurodegener 2011, 6:56
35. Masland RH: Cell populations of the retina: the Proctor lecture. Invest Ophthalmol Vis Sci 2011, 52:4581–4591
36. Finnemann SC, Nandrot EF: MerTK activation during RPE phagocytosis in vivo requires alphaVbeta5 integrin. Adv Exp Med Biol 2006, 572:499–503
37. Taniguchi-Ikeda M, Kobayashi K, Kanagawa M, Yu CC, Mori K, Oda T, Kuga A, Kurahashi H, Akman HO, DiMauro S, Kaji R, Yokota T, Takeda S, Toda T: Pathogenic exon-trapping by SVA retrotransposon and rescue in Fukuyama muscular dystrophy. Nature 2011, 478:127–131
38. Dell'Angelica EC: AP-3-dependent trafficking and disease: the first decade. Curr Opin Cell Biol 2009, 21:552–559
39. Farkas MH, Grant GR, White JA, Sousa ME, Consugar MB, Pierce EA: Transcriptome analyses of the human retina identify unprecedented transcript diversity and 3.5 Mb of novel transcribed sequence via significant alternative splicing and novel genes. BMC Genomics 2013, 14:486
40. Buchholz DE, Pennington BO, Croze RH, Hinman CR, Coffey PJ, Clegg DO: Rapid and efficient directed differentiation of human pluripotent stem cells into retinal pigmented epithelium. Stem Cells Transl Med 2013, 2:384–393
41. Meyer JS, Howden SE, Wallace KA, Verhoeven AD, Wright LS, Capowski EE, Pinilla I, Martin JM, Tian S, Stewart R, Pattnaik B, Thomson JA, Gamm DM: Optic vesicle-like structures derived from human pluripotent stem cells facilitate a customized approach to retinal disease treatment. Stem Cells 2011, 29:1206–1218
42. Singh R, Phillips MJ, Kuai D, Meyer J, Martin JM, Smith MA, Perez ET, Shen W, Wallace KA, Capowski EE, Wright LS, Gamm DM: Functional analysis of serially expanded human iPS cell-derived RPE cultures. Invest Ophthalmol Vis Sci 2013, 54:6767–6778